Precision measurement of $\mathcal{B}(D^+ \to \mu^+\nu)$ and the pseudoscalar decay constant f_{D^+}

B. I. Eisenstein,[1] I. Karliner,[1] S. Mehrabyan,[1] N. Lowrey,[1] M. Selen,[1] E. J. White,[1] J. Wiss,[1] R. E. Mitchell,[2] M. R. Shepherd,[2] D. Besson,[3] T. K. Pedlar,[4] D. Cronin-Hennessy,[5] K. Y. Gao,[5] J. Hietala,[5] Y. Kubota,[5] T. Klein,[5] B. W. Lang,[5] R. Poling,[5] A. W. Scott,[5] P. Zweber,[5] S. Dobbs,[6] Z. Metreveli,[6] K. K. Seth,[6] A. Tomaradze,[6] J. Libby,[7] L. Martin,[7] A. Powell,[7] G. Wilkinson,[7] K. M. Ecklund,[8] W. Love,[9] V. Savinov,[9] H. Mendez,[10] J. Y. Ge,[11] D. H. Miller,[11] I. P. J. Shipsey,[11] B. Xin,[11] G. S. Adams,[12] M. Anderson,[12] J. P. Cummings,[12] I. Danko,[12] D. Hu,[12] B. Moziak,[12] J. Napolitano,[12] Q. He,[13] J. Insler,[13] H. Muramatsu,[13] C. S. Park,[13] E. H. Thorndike,[13] F. Yang,[13] M. Artuso,[14] S. Blusk,[14] S. Khalil,[14] J. Li,[14] N. Menaa,[14] R. Mountain,[14] S. Nisar,[14] K. Randrianarivony,[14] N. Sultana,[14] T. Skwarnicki,[14] S. Stone,[14] J. C. Wang,[14] L. M. Zhang,[14] G. Bonvicini,[15] D. Cinabro,[15] M. Dubrovin,[15] A. Lincoln,[15] P. Naik,[16] J. Rademacker,[16] D. M. Asner,[17] K. W. Edwards,[17] J. Reed,[17] R. A. Briere,[18] T. Ferguson,[18] G. Tatishvili,[18] H. Vogel,[18] M. E. Watkins,[18] J. L. Rosner,[19] J. P. Alexander,[20] D. G. Cassel,[20] J. E. Duboscq,[20] R. Ehrlich,[20] L. Fields,[20] R. S. Galik,[20] L. Gibbons,[20] R. Gray,[20] S. W. Gray,[20] D. L. Hartill,[20] B. K. Heltsley,[20] D. Hertz,[20] J. M. Hunt,[20] J. Kandaswamy,[20] D. L. Kreinick,[20] V. E. Kuznetsov,[20] J. Ledoux,[20] H. Mahlke-Krüger,[20] D. Mohapatra,[20] P. U. E. Onyisi,[20] J. R. Patterson,[20] D. Peterson,[20] D. Riley,[20] A. Ryd,[20] A. J. Sadoff,[20] X. Shi,[20] S. Stroiney,[20] W. M. Sun,[20] T. Wilksen,[20] S. B. Athar,[21] R. Patel,[21] J. Yelton,[21] and P. Rubin[22]

(CLEO Collaboration)

[1]*University of Illinois, Urbana-Champaign, Illinois 61801, USA*
[2]*Indiana University, Bloomington, Indiana 47405, USA*
[3]*University of Kansas, Lawrence, Kansas 66045, USA*
[4]*Luther College, Decorah, Iowa 52101, USA*
[5]*University of Minnesota, Minneapolis, Minnesota 55455, USA*
[6]*Northwestern University, Evanston, Illinois 60208, USA*
[7]*University of Oxford, Oxford OX1 3RH, United Kingdom*
[8]*State University of New York at Buffalo, Buffalo, New York 14260, USA*
[9]*University of Pittsburgh, Pittsburgh, Pennsylvania 15260, USA*
[10]*University of Puerto Rico, Mayaguez, Puerto Rico 00681*
[11]*Purdue University, West Lafayette, Indiana 47907, USA*
[12]*Rensselaer Polytechnic Institute, Troy, New York 12180, USA*
[13]*University of Rochester, Rochester, New York 14627, USA*
[14]*Syracuse University, Syracuse, New York 13244, USA*
[15]*Wayne State University, Detroit, Michigan 48202, USA*
[16]*University of Bristol, Bristol BS8 1TL, United Kingdom*
[17]*Carleton University, Ottawa, Ontario, Canada K1S 5B6*
[18]*Carnegie Mellon University, Pittsburgh, Pennsylvania 15213, USA*
[19]*Enrico Fermi Institute, University of Chicago, Chicago, Illinois 60637, USA*
[20]*Cornell University, Ithaca, New York 14853, USA*
[21]*University of Florida, Gainesville, Florida 32611, USA*
[22]*George Mason University, Fairfax, Virginia 22030, USA*

(Received 12 June 2008; published 11 September 2008)

We measure the branching ratio of the purely leptonic decay of the D^+ meson with unprecedented precision as $\mathcal{B}(D^+ \to \mu^+\nu) = (3.82 \pm 0.32 \pm 0.09) \times 10^{-4}$, using 818 pb^{-1} of data taken on the $\psi(3770)$ resonance with the CLEO-c detector at the CESR collider. We use this determination to derive a value for the pseudoscalar decay constant f_{D^+}, combining with measurements of the D^+ lifetime and assuming $|V_{cd}| = |V_{us}|$. We find $f_{D^+} = (205.8 \pm 8.5 \pm 2.5)$ MeV. The decay rate asymmetry $\frac{\Gamma(D^+\to\mu^+\nu)-\Gamma(D^-\to\mu^-\bar{\nu})}{\Gamma(D^+\to\mu^+\nu)+\Gamma(D^-\to\mu^-\bar{\nu})} = 0.08 \pm 0.08$, consistent with no CP violation. We also set 90% confidence level upper limits on $\mathcal{B}(D^+ \to \tau^+\nu) < 1.2 \times 10^{-3}$ and $\mathcal{B}(D^+ \to e^+\nu) < 8.8 \times 10^{-6}$.

DOI: 10.1103/PhysRevD.78.052003 PACS numbers: 13.20.Fc, 12.38.Qk, 14.40.Lb

I. INTRODUCTION

Purely leptonic decays of heavy mesons involve both weak and strong interactions. The weak part is easy to describe as the annihilation of the quark-antiquark pair via the standard model W^+ boson; the Feynman diagram for $D^+ \to \ell^+\nu$ is shown in Fig. 1. The strong interactions arise due to gluon exchanges between the charm quark and

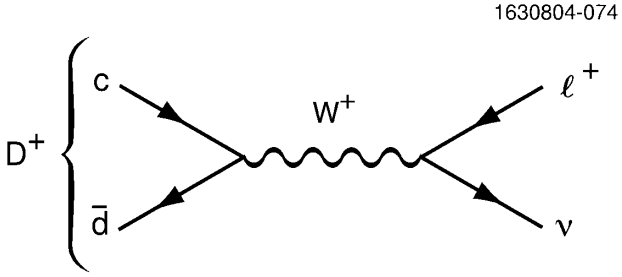

FIG. 1. The decay diagram for $D^+ \to \ell^+ \nu$.

the light quark. These are parametrized in terms of the "decay constant" for the D^+ meson f_{D^+}. The decay rate is given by [1]

$$\Gamma(D^+ \to \ell^+ \nu) = \frac{G_F^2}{8\pi} f_{D^+}^2 m_\ell^2 M_{D^+} \left(1 - \frac{m_\ell^2}{M_{D^+}^2}\right)^2 |V_{cd}|^2, \quad (1)$$

where G_F is the Fermi coupling constant, M_{D^+} is the D^+ mass, m_ℓ is the mass of the final state lepton, and V_{cd} is a Cabibbo-Kobayashi-Maskawa (CKM) matrix element [2], whose magnitude is set equal to 0.2256, the value of V_{us} [3]. Thus, within the context of the standard model (SM), measurement of this purely leptonic decay provides a means of determining f_{D^+}, and similarly measuring the purely leptonic decay of the D_s^+ meson allows us to determine f_{D_s}.

Meson decay constants in the B system are used to translate measurements of $B\bar{B}$ mixing to CKM matrix elements. Currently, it is not possible to determine f_B accurately from leptonic B decays, so theoretical calculations of f_B must be used. Since the B_s meson does not have $\mu\nu$ decays, it will never be possible to determine f_{B_s} experimentally, so again theory must be relied upon. If calculations disagree on D mesons, they may be questionable on B mesons. If, on the other hand new physics is present, it is imperative to understand how it affects SM-based predictions of the B decay constants.

These decay constants can be calculated in theories of QCD. A recent calculation by Follana *et al.* [4] using an unquenched lattice technique predicts $f_{D^+} = (207 \pm 4)$ MeV and $f_{D_s} = (241 \pm 3)$ MeV. The latter result differs by more than 3 standard deviations from the average of CLEO and Belle measurements [5].

Dobrescu and Kronfeld point out that this discrepancy can be caused by the presence of non-SM objects participating virtually in the decay [6]. They give three possibilities: (1) a new boson of charge $+1$ interfering with the SM W^+ annihilation, (2) a charge $+2/3$ leptoquark, and (3) a charge minus $1/3$ leptoquark. The charge $+1$ boson could either be a W'^+ or a charged Higgs. They propose a specific two Higgs doublet model where one doublet gives the c, u and leptons mass, but not the d, s, b, or t, and has a vacuum expectation value of about 2 GeV. Such a model predicts that the ratio of widths $\Gamma(D_s^+ \to \tau^+ \nu)/\Gamma(D_s^+ \to \mu^+ \nu)$ is the same as the standard model expectation, which is in agreement with the CLEO measurements.

The previous CLEO determination of $f_{D^+} = (222.6 \pm 16.7^{+2.3}_{-3.4})$ MeV is consistent with the Follana *et al.* calculation at the 1 standard deviation level, but the experimental error was too large to provide a precision test. Here we provide a measurement based on a 3 times larger data sample and a $\approx 15\%$ larger efficiency based on improved analysis techniques.

One other fully unquenched lattice calculation exists in the literature [7], although it has significantly larger errors than Follana *et al.* [4]. Quenched calculations have also been performed [8–11], and other methods have been used [12–18]. The various theoretical predictions of f_{D^+} range from 190 MeV to 350 MeV. Because of helicity suppression, the electron mode $D^+ \to e^+ \nu$ has a very small rate in the standard model [19]. The expected relative widths are $2.65{:}1{:}2.3 \times 10^{-5}$ for the $\tau^+\nu$, $\mu^+\nu$, and $e^+\nu$ final states, respectively. Unfortunately the mode with the largest branching fraction, $\tau^+\nu$, has at least two neutrinos in the final state and is difficult to detect in D^+ decay.

The CLEO-c detector is equipped to measure the momenta and directions of charged particles, identify charged hadrons, detect photons, and determine their directions and energies with good precision. It has been described in more detail previously [20–23].

II. DATA SAMPLE AND SIGNAL SELECTION

In this study we use 818 pb^{-1} of CLEO-c data collected from e^+e^- collisions at the $\psi(3770)$ resonance. This work contains our previous sample as a subset and supersedes our initial efforts [23]. At this energy, the events consist mostly of pure D^+D^-, $D^0\bar{D}^0$, three-flavor continuum, with small amounts of other final states such as $\gamma\psi(2S)$ and $\tau^+\tau^-$.

We examine all the recorded hadronic events and retain those containing at least one charged D candidate in the modes listed in Table I. We use this sample to look for cases where we have only a single muon candidate whose four-momentum is consistent with a two-body D decay into a muon and a neutrino and no other charged tracks or excess neutral energy are present. Track selection, particle

TABLE I. Tagging modes and numbers of signal and background events determined from the fits shown in Fig. 2.

Mode	Signal	Background
$K^+\pi^-\pi^-$	24 778 ± 497	5957
$K^+\pi^-\pi^-\pi^0$	71 605 ± 359	37 119
$K_S\pi^-$	32 696 ± 189	1576
$K_S\pi^-\pi^-\pi^+$	52 554 ± 315	26 352
$K_S\pi^-\pi^0$	59 298 ± 289	14 837
$K^+K^-\pi^-$	19 124 ± 159	3631
Sum	460 055 ± 787	89 472

identification, π^0, K_S and muon selection criteria are identical to those described in Ref. [23], with one important exception. The angular acceptance of the muon has been widened to cover 90% of the solid angle rather than 81%. Muons deposit less than 300 MeV of energy in the calorimeter 98.8% of the time, while hadrons often interact and deposit significantly more energy. Thus, we define two cases in this paper, where case (i) refers to muon candidate tracks that deposit <300 MeV and case (ii) is for candidates depositing >300 MeV, as was done previously for both our $D^+ \to \tau^+\nu$ and $D_s^+ \to \mu^+\nu$ analyses [24,25]. Briefly, we determine the efficiency on muons from $e^+e^- \to \mu^+\mu^-$ events and compare with our Monte Carlo projection. The excellent agreement allows us to use the Monte Carlo efficiency for the lower energy muons observed in this analysis. Pion's deposit <300 MeV 55% of the time as determined from a relatively pure sample of $D^0 \to K^-\pi^+$ events, and their charge-conjugates.

III. RECONSTRUCTION OF CHARGED D TAGGING MODES

Tagging modes are fully reconstructed by first evaluating the difference in the energy, ΔE, of the decay products with the beam energy. We require the absolute value of this difference to contain 98.8% of the signal events, i.e. to be within ≈ 2.5 times the root mean square (rms) width of the peak value. The rms widths vary from ≈ 7 MeV in the $K^+K^-\pi^-$ mode to ≈ 14 MeV in the $K^+\pi^-\pi^-\pi^0$ mode. For the selected events we then view the reconstructed D^- beam-constrained mass defined as

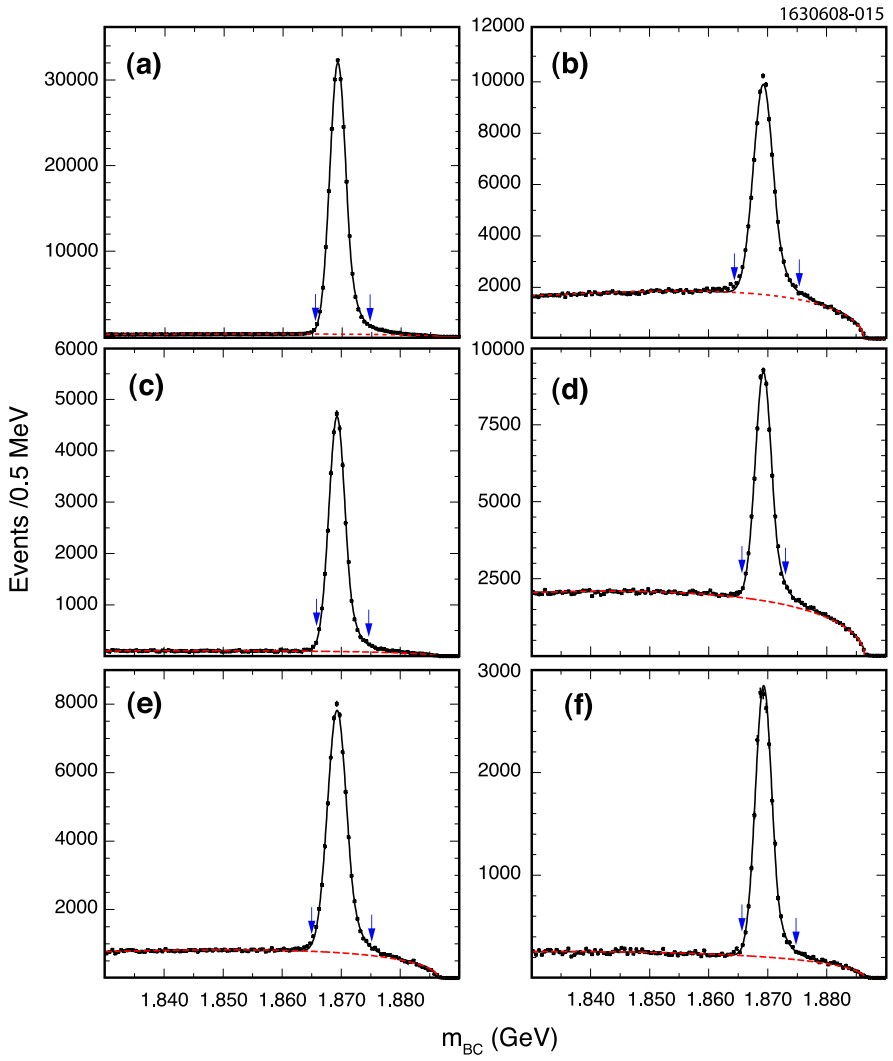

FIG. 2 (color online). Beam-constrained mass distributions for different fully reconstructed D^- decay candidates in the final states: (a) $K^+\pi^-\pi^-$, (b) $K^+\pi^-\pi^-\pi^0$, (c) $K_S\pi^-$, (d) $K_S\pi^-\pi^-\pi^+$, (e) $K_S\pi^-\pi^0$, and (f) $K^+K^-\pi^-$. The solid curves show the sum of signal and background functions. The dashed curves indicate the background fits. The region between the arrows contains the events selected for use in further analysis.

$$m_{\rm BC} = \sqrt{E_{\rm beam}^2 - \left(\sum_i \mathbf{p}_i\right)^2}, \qquad (2)$$

where i runs over all the final state particles of the tag. Since the CESR beams have a crossing angle, we work in the center-of-mass frame. The beam-constrained mass has better resolution than merely calculating the invariant mass of the decay products since the beam has a small energy spread. Besides using D^- tags and searching for $D^+ \to \mu^+\nu$, we also use the charge-conjugate D^+ tags and search for $D^- \to \mu^-\bar{\nu}$; in the rest of this paper we will not usually mention the charge-conjugate modes explicitly, but they are always used.

The $m_{\rm BC}$ distributions for all D^- tagging modes considered in this data sample are shown in Fig. 2. To determine the event numbers we first fit the $m_{\rm BC}$ distributions to a signal function plus a background shape. Then we use the signal shape to define the lower and upper limits in $m_{\rm BC}$, and count the number events above the background function within the limits.

For the background we fit with a shape function analogous to one first used by the ARGUS collaboration [26] which has approximately the correct threshold behavior at large $m_{\rm BC}$. This function is

$$f_{\rm background}(m_{\rm BC}) = a(m_{\rm BC}+b)\sqrt{1-\left(\frac{m_{\rm BC}+b}{c}\right)^2} \times \exp\left[d\left(1-\left[\frac{m_{\rm BC}+b}{c}\right]^2\right)\right], \qquad (3)$$

where a is the overall normalization and b, c, and d are parameters that govern the shape. To fix the shape parameters in each mode, we fit this function to data selected by using ΔE sidebands defined as $5\sigma < |\Delta E| < 7.5\sigma$, where σ is the rms width of the ΔE distribution.

For the signal we use a line shape similar to that used for extracting photon signals from electromagnetic calorimeters, because of the tail towards high mass caused by initial state radiation [27]. The functional form is

$$f_{\rm signal}(m_{\rm BC}) = \begin{cases} A \cdot \exp\left[-\frac{1}{2}\left(\frac{m_{\rm BC}-m_D}{\sigma_{m_{\rm BC}}}\right)^2\right] & \text{for } m_{\rm BC} < m_D - \alpha\cdot\sigma_{m_{\rm BC}} \\ A \cdot \frac{(\frac{n}{\alpha})^n e^{-(1/2)\alpha^2}}{\left(\frac{m_{\rm BC}-m_D}{\sigma_{m_{\rm BC}}}+\frac{n}{\alpha}-\alpha\right)^n} & \text{for } m_{\rm BC} > m_D - \alpha\cdot\sigma_{m_{\rm BC}}. \end{cases} \qquad (4)$$

Here $A^{-1} \equiv \sigma_{m_{\rm BC}} \cdot [\frac{n}{\alpha}\cdot\frac{1}{n-1}e^{-(1/2)\alpha^2} + \sqrt{\frac{\pi}{2}}(1+{\rm erf}(\frac{\alpha}{\sqrt{2}}))]$, $m_{\rm BC}$ is the measured mass, m_D is the "true" (or most likely) mass $\sigma_{m_{\rm BC}}$ is the mass resolution, and α and n are shape parameters.

Table I lists the modes along with the numbers of signal events and background events within the signal region defined as containing 98.8% of the signal events with $m_{\rm BC}$ below the peak and 95.5% of the signal events above the peak.

We retain the events within the mass cuts illustrated in Fig. 2 for further analysis. This sample includes $460\,055 \pm 787 \pm 2760$ signal events, where the last error is systematic. Because of their low multiplicity, it is easier to find tags in simple $\mu^+\nu$ events than in typical D^+D^- events. Therefore, to calculate the branching fraction we increase the number of tags by $(1.54 \pm 0.36)\%$, as determined by Monte Carlo simulation. The systematic error on the signal number includes this uncertainty added in quadrature with the change given by varying the background function.

IV. $D^+ \to \mu^+\nu$ SELECTION CRITERIA

Using our sample of D^- event candidates we search for events with a single additional charged track presumed to be a μ^+. Then we infer the existence of the neutrino by requiring a measured value of the missing mass squared ($\rm MM^2$) near zero (the neutrino mass), where

$$\rm MM^2 = (E_{beam} - E_{\mu^+})^2 - (-\mathbf{p}_{D^-} - \mathbf{p}_{\mu^+})^2, \qquad (5)$$

here $\mathbf{p}_{D^-}$ is the three-momentum of the fully reconstructed D^-, and $E_{\mu^+}(\mathbf{p}_{\mu^+})$ is the energy (momentum) of the candidate μ^+.

To restrict the sample to candidate $\mu^+\nu$ events resulting from the other D, we exclude events with extra neutral energy, or more than one additional track with opposite charge to the tagged D, which we take to be the muon candidate. We allow such extra tracks if their distance of closest approach from the beam collision point is outside a region more than 5 cm along the beam or more than 5 mm perpendicular to the beam; we do not wish to veto these tracks as they are usually due to interactions of the tracks from the tagging D^- in the calorimeter. We reject events with extra fully reconstructed $K_S \to \pi^+\pi^-$ candidates. We also veto events having a maximum neutral energy cluster of more than 250 MeV, consistent with being a photon. This criterion is highly effective in reducing backgrounds especially from $D^+ \to \pi^+\pi^0$ decays. We consider only those showers that do not match a charged track within a connected region. A connected region is a group of adjacent crystals with finite energy depositions. This reduces the probability of a false veto due to hadronic shower fragments that would otherwise show up as unmatched showers.

Sometimes the decay products of the tagging D^- interact in the detector material, mostly the EM calorimeter, and spray tracks and neutral energy back into the rest of the detector. We evaluate the size of these contributions to the

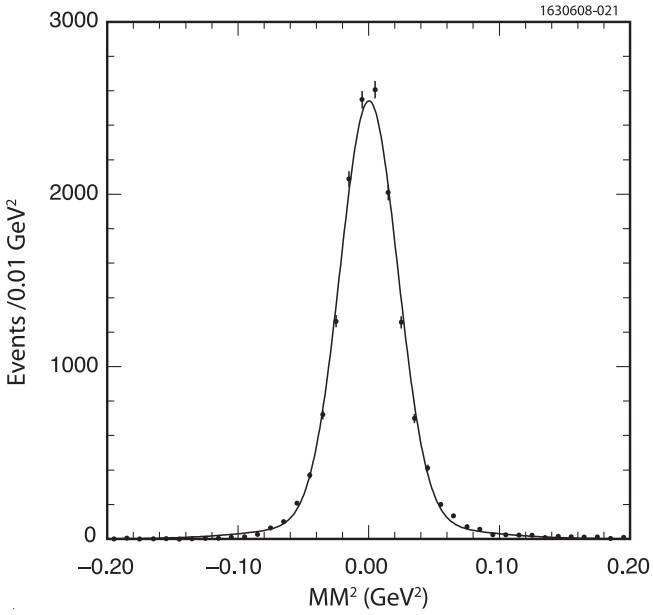

FIG. 3. Monte Carlo simulation of the MM^2 distributions for $D^+ \to \mu^+\nu$ events opposite the proper mixture of tag final states. The fit is to two Gaussian distributions centered at zero where the second Gaussian constitutes around 30% of the area.

inefficiency caused by imposing the 250 MeV extra neutral energy requirement by using fully reconstructed D^+D^- events. We start with events where the $D^+ \to K^-\pi^+\pi^+$ and the $D^- \to K^+\pi^-\pi^-$. We then look for extra photons with energies >250 MeV. This measures the square of the efficiency for the case of $K^-\pi^+\pi^+$ tags, our largest mode. We then measure the inefficiency for each tag mode by looking for fully reconstructed events where one D decays into $K^\mp\pi^\pm\pi^\pm$ and the other into one of the other tag modes. The weighted average over all our tag modes gives an efficiency for our extra energy veto of $(95.9 \pm 0.2 \pm 0.4)\%$. The details are given in Appendix A.

We define θ as the angle with respect to the positron beam direction. The muon candidate direction is required to have $|\cos\theta| < 0.90$, and deposit less than 300 MeV of energy in the calorimeter, characteristic of a minimum ionizing particle.

The MM^2 from the Monte Carlo simulation is shown in Fig. 3 for the proper mix of tag modes. The signal is fit to a sum of two Gaussian distributions with the wider Gaussian having about 30% of the area independent of tagging mode. The average resolution (σ) is defined as

$$\sigma = f_1\sigma_1 + (1 - f_1)\sigma_2, \tag{6}$$

where σ_1 and σ_2 are the individual widths of the two Gaussians and f_1 is the fractional area of the first Gaussian. The resolution of 0.0266 ± 0.0006 GeV^2 is consistent among all the tagging decay modes when restricting the fit range to $-0.2 < MM^2 < 0.2$ GeV^2. In a narrower range, $-0.1 < MM^2 < 0.1$ GeV^2, the resolution is $\sigma = 0.0248 \pm 0.0006$ GeV^2. We use differences in the signal function width to evaluate the systematic error.

We check our simulations by using the $D^+ \to K_S\pi^+$ decay. Here we choose events with the same requirements as used to search for $\mu^+\nu$ but require one additional found K_S. The MM^2 distribution for this final state is shown in Fig. 4(a) and peaks as expected at the K_S mass-squared of 0.25 GeV^2. The resolution depends slightly on the fitting range, which must be specified since the data have a high MM^2 background. In the interval $0.05 < MM^2 < 0.35$ GeV^2, the data show a resolution of $\sigma = 0.0247 \pm 0.0012$ GeV^2, while the Monte Carlo fit gives a consistent value of $\sigma = 0.0235 \pm 0.0007$ GeV^2.

The MM^2 distributions for our tagged events requiring no extra charged tracks besides the muon candidate and no extra showers above 250 MeV as described above are shown in Fig. 5. We see a peak near zero mostly due to the $D^+ \to \mu^+\nu$ mode we are seeking. The large peak centered near 0.25 GeV^2, far from our signal region, results from the decay $D^+ \to \bar{K}^0\pi^+$, and is expected since many K_L escape our detector.

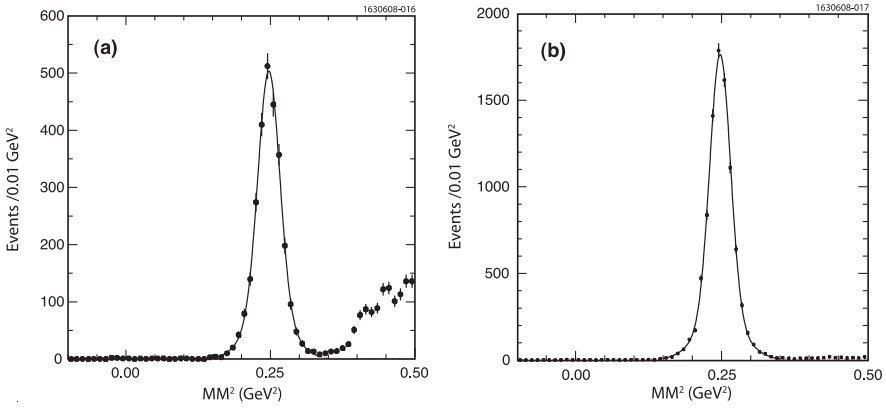

FIG. 4. MM^2 distribution for the decay $D^+ \to K_S\pi^+$ from data (a), and signal Monte-Carlo simulation (b).

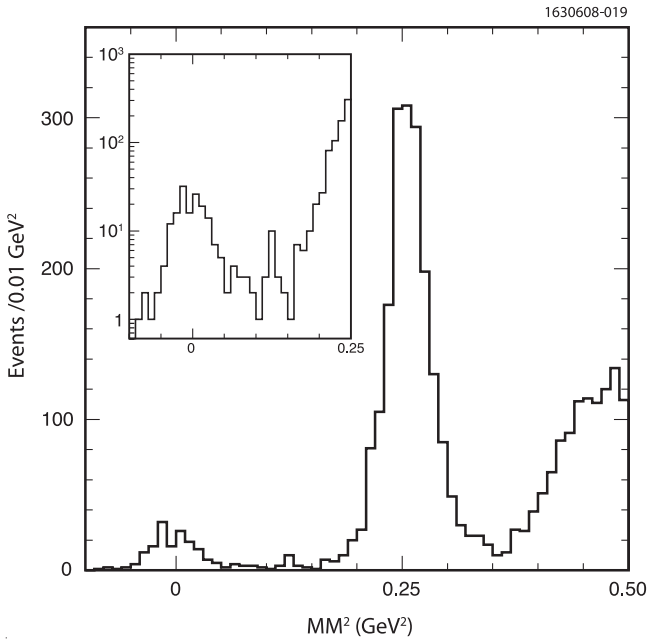

FIG. 5. MM^2 using D^- tags and one additional opposite sign charged track and no extra energetic showers (see text). The insert shows the signal region for $D^+ \to \mu^+\nu$ on a log scale.

V. BACKGROUND CONSIDERATIONS

In this section we will estimate backgrounds from specific sources and also specify shapes of several distinct background distributions. Our procedure will be to fit the signal MM^2 distribution with the sum of the signal and background shapes and then subtract off any residual backgrounds, which we will show are very small. The signal shapes include both the $\mu^+\nu$ and $\tau^+\nu$, $\tau^+ \to \pi^+\nu$ distributions, separately.

There are several background sources we need to evaluate. These include background from other D^+ modes, background from misidentified $D^0\bar{D}^0$ events and continuum background including that from $e^+e^- \to \gamma\psi(2S)$, termed "radiative return." Hadronic sources need to be considered because the requirement of the muon depositing less than 300 MeV in the calorimeter, while 98.8% efficient for muons, rejects only 45% of pions.

We include a calculated background from $D^+ \to \pi^+\pi^0$ in the fit, both the shape and the normalization. This mode is the most difficult to reject because the MM^2 peaks very close to zero, at 0.018 GeV^2, well within our resolution of 0.0266 GeV^2. It is possible for the photons from the π^0 decay to inadvertently be matched to the tracks from the tagging D^- or be missed, even though at least one photon from the $\pi^+\pi^0$ mode exceeds our 250 MeV calorimeter energy requirement and should in most cases cause such a decay to be vetoed. Both the shape in MM^2 and the rate are accurately determined [28]. Using Monte Carlo simulation, we find efficiencies of 1.53% and 1.06%, for the calorimeter energy deposition cases (i) and (ii), respectively. [Recall case (i) is for energies less than 300 MeV, and case (ii) for larger energy depositions.] Multiplying this efficiency by the number of tags and branching ratio, $(1.3 \pm 0.2)\%$, gives a 9.2 event background. The uncertainty in the branching ratio is included in the systematic error.

The $\bar{K}^0\pi^+$ mode gives a large peak in the MM^2 spectrum near 0.25 GeV^2. While it is many standard deviations from our signal region, we need to know the shape of the tail of this distribution. We also need to see if there are any "pathological" events due to non-Gaussian effects. We use the double tag D^0 events where both D's decay into $K^\mp\pi^\pm$ to evaluate both effects. Here we gather a sample of single tag $K^-\pi^+$ decays using strict ΔE and $m_{\rm BC}$ criteria, and look for events with only two oppositely charged tracks where the ring imaging Cherenkov system (RICH) identifies one as a K^+ and other as a π^-. The kaon is required to be in the RICH solid angle but the pion can be anywhere within $|\cos(\theta)| < 0.9$, and then we ignore the kaon. The MM^2 distribution is shown in Fig. 6.

The fit gives us a rather good description of the shape of the $\bar{K}^0\pi^+$ peak, especially on the low MM^2 side, where the $K^0\pi^+\pi^0$ background is absent. There are 2547 $K\pi$ events. The small numbers of residual events peaking near the pion mass squared could be due to $\pi^+\pi^-$ events where the RICH was fooled. The fake rate in the RICH has been well measured as $(1.2 \pm 0.4)\%$ for pions faking kaons in the momentum region of interest (see Appendix B). The relative branching $\mathcal{B}(D^0 \to \pi^+\pi^-)/\mathcal{B}(D^0 \to K^+\pi^-)$ is 3.59% [2]. Thus we expect 1.1 $\pi^+\pi^-$ events. There are three observed events consistent with being in the signal region near MM^2 of zero GeV^2. These three events then

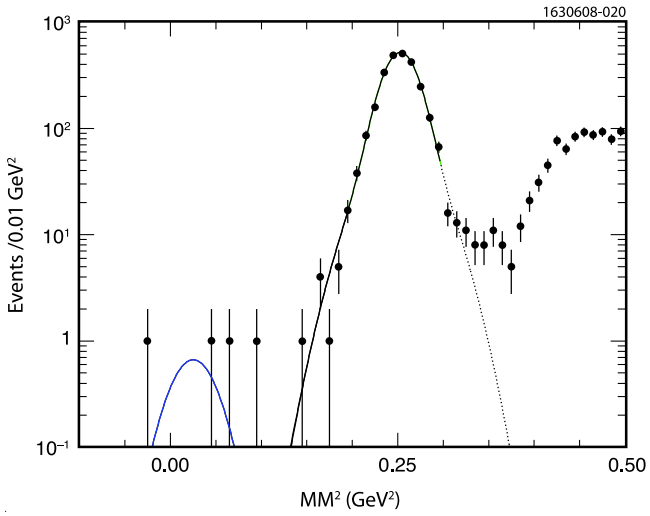

FIG. 6 (color online). The MM^2 from events with $D^0 \to K^-\pi^+$ tag and the other D decaying into two tracks, most likely $\bar{D}^0 \to K^+\pi^-$, where the kaon is ignored. The kaon peak is fit to a double Gaussian distribution, containing 2547 events. The other curve shows the expected shape for $\pi^+\pi^-$.

can be either background associated with $K^+\pi^-$ events or $\pi^+\pi^-$ events. Our best estimate is that 1.9 of them are background. By normalizing the background based on the number of $\bar{K}^0\pi^+$ events in the MM^2 spectrum, we expect 1.3 events as the background from this non-Gaussian effect in case (i) events.

The only significant non-$\mu^+\nu$ population in the signal region arises from $D^+ \to \tau^+\nu$. Out of 10 000 simulated events with D^- tags, we find events in the $\mu^+\nu$ signal region only when $\tau^+ \to \pi^+\nu$. Because of the small D^+-τ^+ mass difference, the τ^+ is almost at rest in the laboratory frame and thus the π^+ has relatively large momentum causing the MM^2 distribution to populate preferentially the low MM^2 region, even though there are two missing neutrinos in this case. Thus, we generate a shape from Monte Carlo specifically for this one decay sequence as shown in Fig. 7.

Other backgrounds from τ^+ decays include additional missing particles. We form a shape consisting of a sum of the τ^+ decay modes $\rho^+\bar{\nu}$, $\mu^+\nu\bar{\nu}$ and other "similar" modes $\rho^+\pi^0$, and $\pi^0\mu^+\nu$. All the relevant branching ratios are known, where we take the $D^+ \to \tau^+\nu$ rate by multiplying our previous $\mu^+\nu$ result by 2.65, the standard model prediction. We use this shape to describe these backgrounds; we do not, however, fix the normalization in the fit.

We have also checked the possibility of other D^+D^- decay modes producing background with an equivalent 1.7 fb^{-1} Monte Carlo sample; we find no additional events. The $D^0\bar{D}^0$ and continuum backgrounds are also evaluated by analyzing Monte Carlo samples corresponding to 4.1 and 3.0 fb^{-1}, respectively. To normalize our Monte Carlo events to our data sample we used $\sigma_{D^0\bar{D}^0} = 3.7$ nb [29] and $\sigma_{\text{continuum}} = 18$ nb. We also found no events in our analysis of a simulated radiative return sample equivalent to 2.7 fb^{-1}. Our total additional background is 2.4 ± 1.0 events, with the individual components listed in Table II.

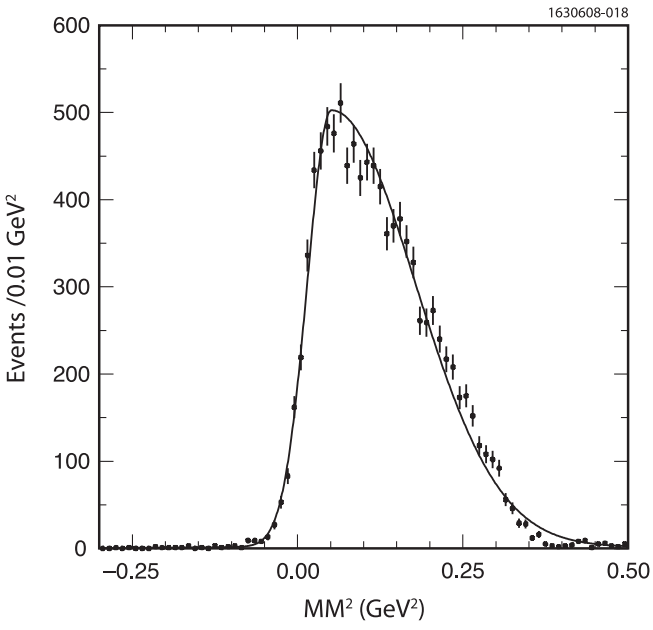

FIG. 7. The simulated MM^2 from $D^+ \to \tau^+\nu$, $\tau^+ \to \pi^+\nu$ fit to the sum of two Gaussian distributions, whose widths are allowed to vary on both sides of their respective maximums.

TABLE II. Backgrounds from additional sources, not contained in the fitting functions.

Mode	# of Events
Continuum	0.8 ± 0.4
$\bar{K}^0\pi^+$	1.3 ± 0.9
D^0 modes	0.3 ± 0.3
Sum	2.4 ± 1.0

VI. BRANCHING RATIO AND DECAY CONSTANT

We preform a binned maximum likelihood fit to the case (i) MM^2 distribution up to a MM^2 of 0.28 GeV^2. Beyond that value other final states such as $\eta\pi^+$ and $K^0\pi^+\pi^0$ begin to contribute. The fit shown in Fig. 8 contains

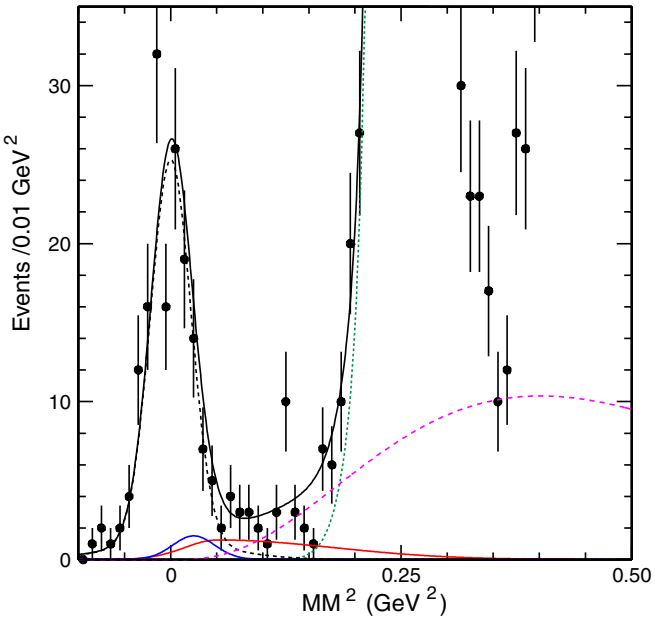

FIG. 8 (color online). Fit to the MM^2 for case (i). Here the ratio of $\tau^+\nu$, $\tau^+ \to \pi^+\bar{\nu}$ to $\mu^+\nu$ events is fixed to the SM value. The points with error bars show the data. The black (dashed) curve centered at zero shows the signal $\mu^+\nu$ events. The dot-dashed (red) curve that peaks around 0.05 GeV^2 shows the $D^+ \to \tau^+\nu$, $\tau^+ \to \pi^+\bar{\nu}$ component. The solid (blue) Gaussian shaped curve centered on the pion-mass squared shows the residual $\pi^+\pi^0$ component. The dashed (purple) curve that falls to zero around 0.03 GeV^2 is the sum of all the other background components, except the $\bar{K}^0\pi^+$ tail which is shown by the long-dashed (green) curve that peaks up at 0.25 GeV^2. The solid (black) curve is the sum of all the components.

separate shapes for signal, $\pi^+\pi^0$, $\bar{K}^0\pi^+$, $\tau^+\nu$ ($\tau^+ \to \pi^+\bar{\nu}$), and the background cocktail described above. Here we assume the standard model ratio of 2.65 for the ratio of the $\tau^+\nu/\mu^+\nu$ component and constrain the area ratio of these components to the product of 2.65 with $\mathcal{B}(\tau^+ \to \pi^+\bar{\nu}) = (10.90 \pm 0.07)\%$ [2] and the 55% probability that the pion deposits <300 MeV in the calorimeter. The normalization of the $\pi^+\pi^0$ component is also fixed at 9.2 events, the product of the number of tags, times the branching fraction, times the 1.53% detection efficiency. The normalization of the additional background shape described above is allowed to float.

The fit yields 149.7 ± 12.0 $\mu^+\nu$ signal events and 25.8 $\tau^+\nu$, $\tau^+ \to \pi^+\bar{\nu}$ events (for the entire MM^2 range). We can also perform the fit allowing the $\tau^+\nu$, $\tau^+ \to \pi^+\bar{\nu}$ component to float. (See Fig. 9.) Then we find 153.9 ± 13.5 $\mu^+\nu$ events and 13.5 ± 15.3 $\tau^+\nu$, $\tau^+ \to \pi^+\bar{\nu}$ events,

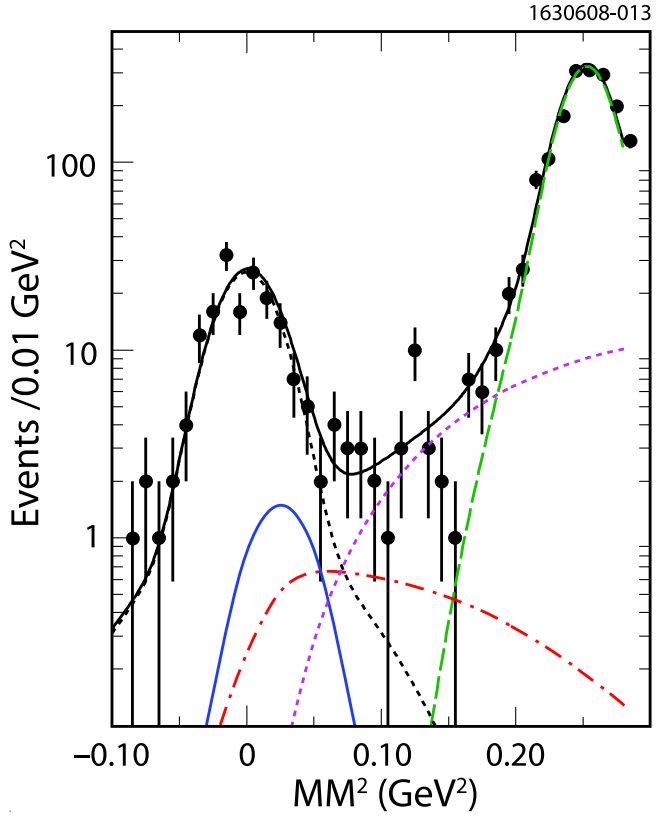

FIG. 9 (color online). Fit to the MM^2 for case (i) allowing the $\tau^+\nu$, $\tau^+ \to \pi^+\bar{\nu}$ component to float. The points with error bars show the data. The black (dashed) curve centered at zero shows the signal $\mu^+\nu$ events. The dot-dashed (red) curve that peaks around 0.05 GeV^2 shows the $D^+ \to \tau^+\nu$, $\tau^+ \to \pi^+\bar{\nu}$ component. The solid (blue) Gaussian shaped curve centered on the pion-mass squared shows the residual $\pi^+\pi^0$ component. The dashed (purple) curve that falls to zero around 0.03 GeV^2 is the sum of all the other background components, except the $\bar{K}^0\pi^+$ tail which is shown by the long-dashed (green) curve that peaks up at 0.25 GeV^2. The solid (black) curve is the sum of all the components.

compared with the 25.8 we expect in the standard model. Performing the fit in this manner gives a result that is independent of the SM expectation of the $D^+ \to \tau^+\nu$ rate. To extract a branching fraction, in either case, we subtract off the 2.4 ± 1.0 events determined above to be additional backgrounds, not taken into account by the fit, and divide by the product of the efficiency and the number of tags.

The detection efficiency of 81.8% for the single muon includes the tracking and particle identification efficiencies, the probability of the crystal energy being less than 300 MeV, and the 95.9% efficiency of not having another unmatched shower in the event with energy greater than 250 MeV; the latter is determined from the data presented in Table V of Appendix A. The systematic errors on the branching ratio are listed in Table III.

The systematic error on the MM^2 fit is determined by changing the signal shape and the fitting range. The difference in signal shapes between the $K_S\pi^+$ data and Monte Carlo is 0.0012 ± 0.0014 GeV^2. We refit the case (i) data while increasing σ by 0.0012 GeV^2, 0.0024 GeV^2, and finally letting σ float. (We fix the $\tau^+\nu/\mu^+\nu$ ratio.) The resulting numbers of events change from our baseline by $+0.41$, $+0.79$ and $+0.26$ events, respectively. This allows us to set the 0.2% systematic error from this source.

The track finding and particle identification efficiencies associated with the single muon are determined by comparing selected samples formed using partial reconstruction [30] to the Monte Carlo simulation. We include the particle identification because we do veto identified kaons as muon candidates.

A check of the background is provided by considering case (ii), where more than 300 MeV is deposited in the calorimeter by the muon candidate track. Only 1.2% of muons pass such a requirement. We fit this sample as in case (i), but here fixing both the $\mu^+\nu$ and the $\tau^+\nu$ contributions from the case (i) fit (with the ratio of the two fixed). The normalizations of the $K^0\pi^+$ tail and the background shape are allowed to float. The fit is shown in Fig. 10. The number of events in the signal region, MM$^2 \leq 0.05$ GeV^2, is 1.7, fixed from the $\mu^+\nu$ sample, 5.4 fixed

TABLE III. Systematic errors on the $D^+ \to \mu^+\nu$ branching ratio.

	Systematic errors (%)
Track finding	0.7
PID cut	1.0
MM^2 width	0.2
Minimum ionization cut	1.0
Number of tags	0.6
Extra showers cut	0.4
Radiative corrections	1.0
Background	0.7
Total	2.2

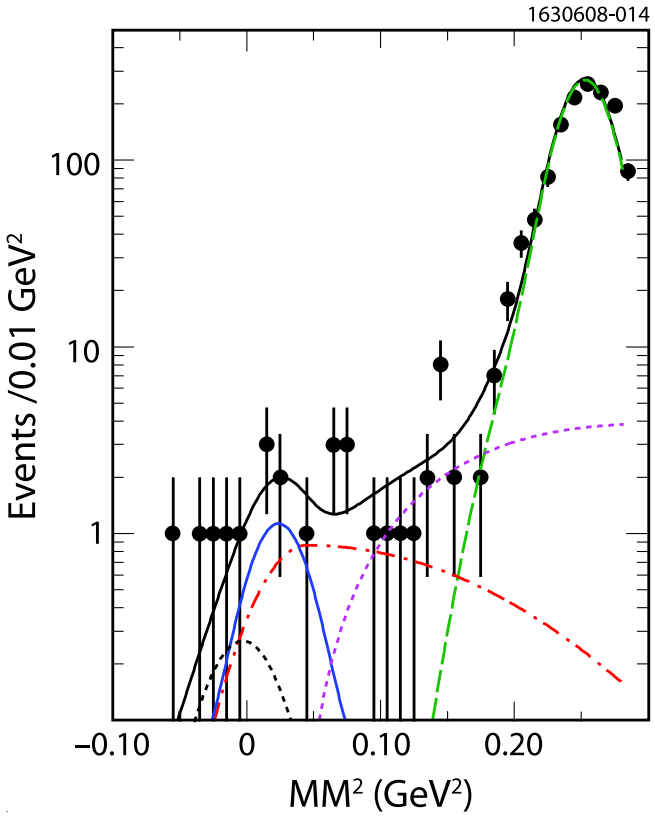

FIG. 10 (color online). Fit to the MM^2 for case (ii) which has little $\mu^+\nu$ signal contribution, and tests our understanding of the background. The points with error bars show the data. The $\mu^+\nu$ component, the black (dashed) curve (almost invisibly small) shows the signal $\mu^+\nu$ events fixed from the case (i) fit. The points with error bars show the data. The dot-dashed (red) curve that peaks around 0.05 GeV^2 shows the $D^+ \to \tau^+\nu$, $\tau^+ \to \pi^+\bar{\nu}$ component. The solid (blue) Gaussian shaped curve centered on the pion-mass squared shows the residual $\pi^+\pi^0$ component. The dashed (purple) curve that falls to zero around 0.03 GeV^2 is the sum of all the other background components, except the $\bar{K}^0\pi^+$ tail which is shown by the long-dashed (green) curve that peaks up at 0.25 GeV^2. The solid (black) curve is the sum of all the components.

from the $\pi^+\pi^0$, and 4.0 from the $\tau^+\nu$. This sums to 11.1 events, while we count 11 events in this region. Thus we have an excess of -0.1 ± 3.3 events, which is consistent with our other background estimate of 2.4 ± 1.0 events and gives us confidence in using this estimate.

The branching fraction determined from fixing the $\tau^+\nu$ contribution relative to the $\mu^+\nu$, is

$$\mathcal{B}(D^+ \to \mu^+\nu) = (3.82 \pm 0.32 \pm 0.09) \times 10^{-4}. \quad (7)$$

The decay constant f_{D^+} is then obtained from Eq. (1) using 1040 ± 7 fs as the D^+ lifetime [2] and 0.2256 as $|V_{cd}|$ [3]. Our final result is

$$f_{D^+} = (205.8 \pm 8.5 \pm 2.5)\ \text{MeV}. \quad (8)$$

A somewhat less precise value is obtained by floating the $\tau^+\nu$ to $\mu^+\nu$ ratio. That fit gives

$$\mathcal{B}(D^+ \to \mu^+\nu) = (3.93 \pm 0.35 \pm 0.09) \times 10^{-4}. \quad (9)$$

The corresponding value of the decay constant is

$$f_{D^+} = (207.6 \pm 9.3 \pm 2.5)\ \text{MeV}. \quad (10)$$

The former value is the most precise measurement in the context of the standard model, while the latter does not use any standard model assumptions. In both cases the additional systematic errors due to the D^+ lifetime measurement and the error on $|V_{cd}| = |V_{us}|$ are negligible.

The data have already been corrected for final state radiation of the muon, as our Monte Carlo simulation incorporates this effect [31]. There is however, another process where the $D^+ \to \gamma D^{*+} \to \gamma\mu^+\nu$, where the D^{*+} is a virtual vector or axial-vector meson. The $D^{*+} \to \mu^+\nu$ transition is not helicity-suppressed, so the factor α for radiation is compensated by a relative factor $(M_{D^+}/m_\mu)^2$. Using Eq. (12) of Burdman *et al.* [32] and imposing the 250 MeV photon cut, we find that the radiative rate is approximately 1%, to which we assign a $\pm 1\%$ systematic error. This is essentially the same calculation done by Dobrescu and Kronfeld for $D_s^+ \to \mu^+\nu$ decays [6]. (The results shown above for the branching fractions and f_{D^+} are all radiatively corrected; the branching fractions have been reduced by 1%.)

VII. SEARCH FOR $D^+ \to \tau^+\nu$

We also use our data to perform a search for the $\tau^+\nu$ final state. Here we do a simultaneous binned maximum likelihood fit to both the case (i) and case (ii) data fixing the ratio of the $\tau^+\nu$ final state to be 55/45 in the two cases, determined by the relative acceptances for the 300 MeV calorimeter energy requirement. The fits are shown in Fig. 11.

The fit yields a sum of 27.8 ± 16.4 $\tau^+\nu$, $\tau^+ \to \pi^+\bar{\nu}$ events for the entire MM^2 range. To be conservative in setting an upper limit, we assume all events are signal and do not subtract additional backgrounds from this yield. We include the small systematic errors from the fitting procedure in our calculations. We find

$$\mathcal{B}(D^+ \to \tau^+\nu) < 1.2 \times 10^{-3} \quad (11)$$

at 90% confidence level, and the ratio to the $\mu^+\nu$ rate divided by the standard model expectation of 2.65 is

$$\frac{\Gamma(D^+ \to \tau^+\nu)}{2.65 \cdot \Gamma(D^+ \to \mu^+\nu)} < 1.2 \quad (12)$$

also at 90% confidence level.

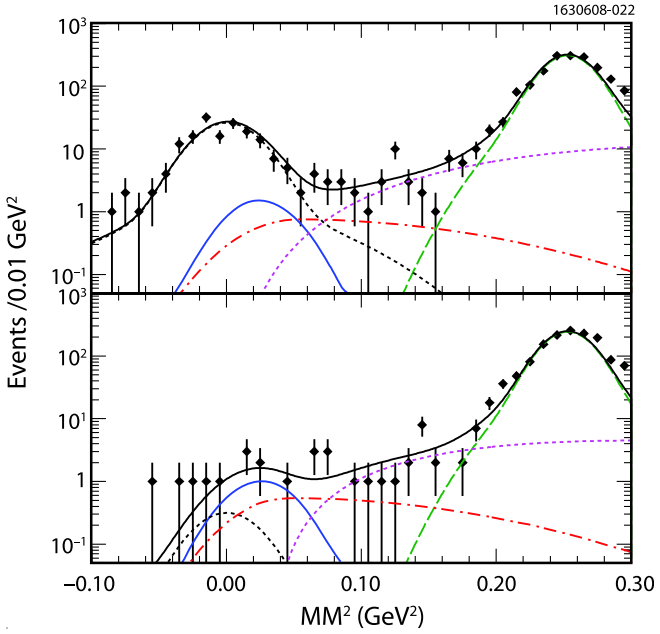

FIG. 11 (color online). Fit to the MM^2 for cases (i) (top) and (ii) (bottom) with the $\tau^+\nu$ components fixed in the ratio 55/45. The points with error bars show the data. The black (dashed) curve centered at zero shows the signal $\mu^+\nu$ events. The dot-dashed (red) curve that peaks around 0.05 GeV^2 shows the $D^+ \to \tau^+\nu$, $\tau^+ \to \pi^+\bar{\nu}$ component. The solid (blue) Gaussian shaped curve centered on the pion-mass squared shows the residual $\pi^+\pi^0$ component. The dashed (purple) curve that falls to zero around 0.03 GeV^2 is the sum of all the other background components, except the $\bar{K}^0\pi^+$ tail which is shown by the long-dashed (green) curve that peaks up at 0.25 GeV^2. The solid (black) curve is the sum of all the components.

VIII. SEARCH FOR D^+ DECAY INTO AN POSITRON PLUS NEUTRINO

We use the same tag sample. Candidate positrons are selected on the basis of a likelihood ratio constructed from three inputs: the ratio between the energy deposited in the calorimeter and the momentum measured in the tracking system, the specific ionization dE/dx measured in the drift chamber, and RICH information. Other criteria remain the same, except that we require that the positron candidate track be in the calorimeter barrel with $|\cos\theta| < 0.81$. We do not find any candidates allowing us to set a limit

$$\mathcal{B}(D^+ \to e^+\nu) < 8.8 \times 10^{-6} \quad \text{at 90\%c.l.}, \tag{13}$$

which is 3 orders of magnitude above the SM prediction.

IX. CONCLUSIONS

The result shown here represents the only precision measurement of the pseudoscalar decay constant f_{D^+}. We have significantly improved our previous results. The statistical error has been reduced by almost a factor of 2. The systematic errors remain small. This result uses all the CLEO-c data collected at the $\psi(3770)$ and, as such, all previous results are superseded.

The branching fraction, assuming the standard model ratio for $\tau^+\nu/\mu^+\nu$ is

$$\mathcal{B}(D^+ \to \mu^+\nu) = (3.82 \pm 0.32 \pm 0.09) \times 10^{-4}, \tag{14}$$

and the decay constant is

$$f_{D^+} = (205.8 \pm 8.5 \pm 2.5)\ \text{MeV}. \tag{15}$$

If, on the other hand, we allow the $\tau^+\nu$ contribution to float, we find

$$\mathcal{B}(D^+ \to \mu^+\nu) = (3.93 \pm 0.35 \pm 0.09) \times 10^{-4}. \tag{16}$$

The corresponding value of the decay constant is

$$f_{D^+} = (207.6 \pm 9.3 \pm 2.5)\ \text{MeV}. \tag{17}$$

These results are all radiatively corrected.

Our new values are consistent with our previous measurement [23], as well as the upper limit set by Mark III [33], and the results based on reported yields of 1 and 2.7 events from BES I and II [34], respectively. We also determine $f_{D_s}/f_{D^+} = 1.326 \pm 0.075$, using the world average value of absolute measurements for $D_s^+ \to \ell^+\nu$ as compiled by Rosner and Stone [5], where we include the radiative correction also on the D_s^+ rate.

Our result for f_{D^+}, is consistent with the most accurate unquenched lattice QCD (LQCD) calculation of Follana *et al.* who give a value of (207 ± 4) MeV. This implies that the somewhat greater than 3 standard deviation discrepancy of the experimental measurements of $f_{D_s} = (273 \pm 10)$ MeV [5] with the Follana *et al.* prediction of (241 ± 3) MeV cannot be explained by how they handle the charm quark in their calculation. In fact, since the s quark is heavier than the d quark, it should be easier for lattice calculations to predict f_{D_s} than f_{D^+} [35]. It may be the case that physics beyond the standard model is raising the value of f_{D_s} in one of the ways suggested by Dobrescu and Kronfeld [6], or via R-parity violating supersymmetry [36]. Other standard model based predictions are listed in Table IV.

It is possible in some models of new physics that there is a difference in the $\mu\nu$ decay rate between D^+ and D^- mesons, due to a CP violating interaction [37]. Separating our data into these two classes we find 228 945 ± 551 D^+ tags and 231 107 ± 552 D^- tags. Fitting the data by fixing the relative $\tau^\pm\nu$, $\tau^\pm \to \pi^\pm\nu$ contribution relative to $\mu^\pm\nu$, we find 76.0 ± 8.6 $\mu^+\nu$ events and 64.8 ± 8.1 $\mu^-\nu$ events. The resulting CP violating asymmetry is

$$A_{\text{CP}} \equiv \frac{\Gamma(D^+ \to \mu^+\nu) - \Gamma(D^- \to \mu^-\bar{\nu})}{\Gamma(D^+ \to \mu^+\nu) + \Gamma(D^- \to \mu^-\bar{\nu})} = 0.08 \pm 0.08. \tag{18}$$

At 90% confidence level the limits are $-0.05 < A_{\text{CP}} < 0.21$.

TABLE IV. Theoretical predictions of f_{D^+} and $f_{D_s^+}/f_{D^+}$.

Theory	f_{D^+} (MeV)	$f_{D_s^+}/f_{D^+}$
LQCD (HPQCD + UKQCD) [4]	207 ± 4	1.164 ± 0.011
LQCD (Fermilab + MILC) [7]	$201 \pm 3 \pm 17$	$1.24 \pm 0.02 \pm 0.07$
QL (QCDSF) [8]	$206 \pm 6 \pm 3 \pm 22$	$1.07 \pm 0.02 \pm 0.02$
QL (Taiwan) [9]	$235 \pm 8 \pm 14$	$1.13 \pm 0.03 \pm 0.05$
QL (UKQCD) [10]	$210 \pm 10^{+17}_{-16}$	$1.13 \pm 0.02^{+0.04}_{-0.02}$
QL [11]	$211 \pm 14^{+2}_{-12}$	1.10 ± 0.02
QCD sum rules [12]	177 ± 21	$1.16 \pm 0.01 \pm 0.03$
QCD sum rules [13]	203 ± 20	1.15 ± 0.04
Field correlators [14]	210 ± 10	1.24 ± 0.03
QCD sum rules [15]	195 ± 20	
Relativistic quark model [16]	234	1.15
Potential model [17]	238	1.01
Isospin mass splittings [18]	262 ± 29	

We do not find positive evidence of the decay $D^+ \to \tau^+ \nu$. Our limit is

$$\mathcal{B}(D^+ \to \tau^+ \nu) < 1.2 \times 10^{-3} \tag{19}$$

at 90% confidence level, and the ratio to the $\mu^+ \nu$ rate, divided by the standard model expectation of 2.65 is

$$\frac{\Gamma(D^+ \to \tau^+ \nu)}{2.65 \cdot \Gamma(D^+ \to \mu^+ \nu)} < 1.2 \tag{20}$$

also at 90% confidence level.

Some nonstandard models predict significant rates for the helicity-suppressed decay $D^+ \to e^+ \nu$ [38]. Our upper limit of 8.8×10^{-6} at 90% c.l. restricts these models.

ACKNOWLEDGMENTS

We gratefully acknowledge the effort of the CESR staff in providing us with excellent luminosity and running conditions. D. Cronin-Hennessy and A. Ryd thank the A. P. Sloan Foundation. This work was supported by the National Science Foundation, the U.S. Department of Energy, the Natural Sciences and Engineering Research Council of Canada, and the U.K. Science and Technology Facilities Council. We thank C. Davies, A. Kronfeld, P. Lepage, P. Mackenzie, R. Van de Water, and R. Zwicky for useful discussions.

APPENDIX A: DETERMINATION OF THE EFFICIENCY OF THE 250 MEV CRITERIA ON ADDITIONAL PHOTONS

Although we do not expect more than a few percent inefficiency due to rejecting events with an additional neutral energy cluster >250 MeV, we do not want to incur a large systematic error due to this potential source. Therefore we perform a full five-constraint kinematic fit to the double tag event samples, where one D decays into $K^\mp \pi^\pm \pi^\pm$ and the other into one of the other tag modes. The constraints are that the total energy sum to twice the beam energy, the total three momentum be zero, and the invariant masses of the two D candidates be equal. We do not require them to equal the known D^+ mass. The result of this fit is a common D candidate mass and a χ^2. Restricting our samples to low χ^2 virtually eliminates all backgrounds at the expense of some signal. Specifically, we require that the probability of χ^2, for five constraints be greater than 1%, which eliminates 32% of all event candidates. The numbers of events in the decay modes we use are listed in Table V.

To first order the fully reconstructed $D^+ D^- \to (K^+ \pi^- \pi^-)\,(K^- \pi^+ \pi^+)$ can be considered the superposition of two single tag $D^+ \to \mu^+ \nu$ candidate events where the single tag is $K^+ \pi^- \pi^-$. Then the efficiency of the

TABLE V. Numbers of $D^+ D^-$ events and the efficiency for the first mode when an extra photon >250 MeV is also required.

Mode 1	Mode 2	Events	$N_{\rm lost}(E_{\gamma>250\ \rm MeV})$	$\epsilon_{250}(\%)$ of Mode 1
$K^+ \pi^- \pi^-$	$K^- \pi^+ \pi^+$	4389	431	95.0 ± 0.2
$K^+ \pi^- \pi^- \pi^0$	$K^- \pi^+ \pi^+$	2590	208	96.8 ± 0.6
$K_S \pi^-$	$K^- \pi^+ \pi^+$	1255	112	95.9 ± 0.8
$K_S \pi^- \pi^- \pi^+$	$K^- \pi^+ \pi^+$	1885	153	96.8 ± 0.7
$K_S \pi^- \pi^0$	$K^- \pi^+ \pi^+$	2648	205	97.7 ± 0.5
$K^+ K^- \pi^-$	$K^- \pi^+ \pi^+$	714	75	94.2 ± 1.1
Weighted average				95.9 ± 0.2

TABLE VI. Results of RICH identification on double tag events. RS indicates right sign and WS indicates wrong sign events.

Mode	No ID		Single K		Single π		Double ID	
	(RS)	(WS)	(RS)	(WS)	(RS)	(WS)	(RS)	(WS)
$K^-\pi^+; K^\pm\pi^\mp$	1896	914	1717	11	1846	24	1673	1

250 MeV cut in the $K\pi\pi$ mode is given by

$$\epsilon_{250}^{K\pi\pi} = \sqrt{(1 - N_{\rm lost}/N_{K\pi\pi-K\pi\pi})}. \quad \text{(A1)}$$

We then combine the large and precise $K^-\pi^+\pi^+$ mode with each of the other tags in turn, where

$$\epsilon_{250}^{\rm mode} = (1 - N_{\rm lost}/N_{K\pi\pi-{\rm mode}})/\epsilon_{250}^{K\pi\pi}. \quad \text{(A2)}$$

This method ensures that the number of interactions of particles with material is the same as in the tag sample used for the $\mu^+\nu$ analysis.

The results are listed in Table V. The numbers of events listed are those with a χ^2 cut applied. The overall efficiency for accepting the double tag event requiring that there not be any photons above 250 MeV is given along with the derived efficiency for each mode. The weighted average over all of our tag modes is $(95.9 \pm 0.2 \pm 0.4)\%$. The systematic error arises only from the consideration that we have analyzed a situation corresponding to two overlapping tags rather than one tag plus a muon.

APPENDIX B: RICH PARTICLE IDENTIFICATION EFFICIENCIES

For two-body decays of D mesons, most of the particle identification ability in CLEO comes from the RICH detector. Information on the angle of detected Cherenkov photons is translated into a likelihood of a given photon being due to a particular particle. Contributions from all photons associated with a particular track are then summed to form an overall likelihood denoted as $\mathcal{L}_i$ for each particle hypothesis. To differentiate between pion and kaon candidates, we use the difference: $-2\log(\mathcal{L}_\pi) + 2\log(\mathcal{L}_K)$. A value of zero is used to distinguish between the two possibilities. We require a minimum of three Cherenkov photons.

Here we use a selected sample of $D^0\bar{D}^0 \to K^\mp\pi^\pm + K^\pm\pi^\mp$ decays. We use $-0.0194 < \Delta E < 0.0175$ GeV and $1.8617 < m_{\rm BC} < 1.8673$ GeV for both candidates. This is essentially a background free sample. We expect only $K^-\pi^+K^+\pi^-$ decays since doubly Cabibbo suppressed decays are forbidden due to quantum correlations and the mixing rate as measured is small enough not to allow us to see any events. The momentum distribution of the tracks is flat between 700 MeV/c and 1 GeV/c.

The results are shown in Table VI. The first column labeled "No ID" gives the number of $K^-\pi^+; K^+\pi^-$ pairs called right sign (RS) and the number of $K^-\pi^+; K^-\pi^+$ (or $K^+\pi^-; K^+\pi^-$) pairs that are wrong sign (WS) using only the kinematical constraints of ΔE and $m_{\rm BC}$ given above. The subsequent columns show the results of applying the RICH particle identification criterion to identify only the kaons, only the pions and then both kaons and pions.

The relevant results are summarized as:

(i) The pion efficiency is $(97.3 \pm 0.3)\%$.

(ii) The kaon efficiency is $(90.6 \pm 0.7)\%$.

(iii) The rate of pions faking kaons is $(1.2 \pm 0.4^{+0}_{-0.1})\%$.

(iv) The rate of kaons faking pions is $(2.6 \pm 0.5^{+0}_{-0.1})\%$.

The one doubly identified wrong sign event could be a mixed event, although that is rather unlikely. We use it to assign a negative systematic error on the fake rates in case there is background in our sample.

[1] D. Silverman and H. Yao, Phys. Rev. D **38**, 214 (1988).
[2] W.-M. Yao *et al.*, J. Phys. G **33**, 1 (2006).
[3] We assume that $|V_{cd}|$ equals $|V_{us}|$ and take the value from M. Antonelli, arXiv:0712.0734.
[4] E. Follana *et al.* (HPQCD and UKQCD Collaborations), Phys. Rev. Lett. **100**, 062002 (2008).
[5] J. L. Rosner and S. Stone, arXiv:0802.1043.
[6] B. A. Dobrescu and A. S. Kronfeld, Phys. Rev. Lett. **100**, 241802 (2008).
[7] C. Aubin *et al.* (FNAL Lattice, HPQCD, and MILC), Phys. Rev. Lett. **95**, 122002 (2005).
[8] A. Ali Khan *et al.* (QCDSF Collaboration), Phys. Lett. B **652**, 150 (2007).
[9] T. W. Chiu *et al.*, Phys. Lett. B **624**, 31 (2005).
[10] L. Lellouch and C.-J. Lin (UKQCD), Phys. Rev. D **64**, 094501 (2001).
[11] D. Becirevic *et al.*, Phys. Rev. D **60**, 074501 (1999).
[12] J. Bordes, J. Peñarrocha, and K. Schilcher, J. High Energy Phys. 11 (2005) 014.
[13] S. Narison, arXiv:hep-ph/0202200.
[14] A. M. Badalian *et al.*, Phys. Rev. D **75**, 116001 (2007); see also A. M. Badalian and B. L. G. Bakker, arXiv:hep-ph/0702229.
[15] A. Penin and M. Steinhauser, Phys. Rev. D **65**, 054006 (2002).
[16] D. Ebert, R. N. Faustov, and V. O. Galkin, Phys. Lett. B

635, 93 (2006); D. Ebert *et al.*, Mod. Phys. Lett. A **17**, 803 (2002).
[17] Z. G. Wang *et al.*, Nucl. Phys. **A744**, 156 (2004); L. Salcedo *et al.*, Braz. J. Phys. **34**, 297 (2004).
[18] J. Amundson *et al.*, Phys. Rev. D **47**, 3059 (1993).
[19] Nonstandard models predict different ratios; see for example A. G. Akeroyd and S. Recksiegel, Phys. Lett. B **554**, 38 (2003).
[20] D. Peterson *et al.*, Nucl. Instrum. Methods Phys. Res., Sect. A **478**, 142 (2002).
[21] M. Artuso *et al.*, Nucl. Instrum. Methods Phys. Res., Sect. A **502**, 91 (2003).
[22] Y. Kubota *et al.* (CLEO), Nucl. Instrum. Methods Phys. Res., Sect. A **320**, 66 (1992).
[23] M. Artuso *et al.* (CLEO), Phys. Rev. Lett. **95**, 251801 (2005); G. Bonvicini *et al.* (CLEO), Phys. Rev. D **70**, 112004 (2004).
[24] P. Rubin *et al.* (CLEO), Phys. Rev. D **73**, 112005 (2006).
[25] T. K. Pedlar *et al.* (CLEO), Phys. Rev. D **76**, 072002 (2007).
[26] H. Albrecht *et al.* (ARGUS), Phys. Lett. B **229**, 304 (1989).
[27] T. Skwarnicki, Report No. DESY F31-86-02 (thesis, unpublished) (1986).
[28] K. Arms *et al.* (CLEO), Phys. Rev. D **69**, 071102 (2004).
[29] S. Dobbs *et al.* (CLEO), Phys. Rev. D **76**, 112001 (2007).
[30] See Ref. [29]. The actual values used here are larger because the momentum spectrum is different.
[31] E. Barberio and Z. Was, Comput. Phys. Commun. **79**, 291 (1994), version 2.15 with interference enabled.
[32] G. Burdman, J. T. Goldman, and D. Wyler, Phys. Rev. D **51**, 111 (1995).
[33] J. Adler *et al.* (Mark III), Phys. Rev. Lett. **60**, 1375 (1988); **63**, 1658(E) (1989).
[34] J. Z. Bai *et al.* (BES), Phys. Lett. B **429**, 188 (1998); M. Ablikim *et al.* (BES), Phys. Lett. B **610**, 183 (2005).
[35] A. Kronfeld, P. Mackenzie, and R. Van de Water (private communication).
[36] A. Kundu and S. Nandi, arXiv:0803:1898.
[37] R. Zwicky, Phys. Rev. D **77**, 036004 (2008).
[38] A. G. Akeroyd and S. Recksiegel, Phys. Lett. B **549**, 314 (2002) and references contained therein.